ADVANCED HEALTHCARE MATERIALS
www.advhealthmat.de

Targeted Delivery of the Pan-Inflammasome Inhibitor MM01 as an Alternative Approach to Acute Lung Injury Therapy

Alba García-Fernández, Mónica Sancho, Eva Garrido, Viviana Bisbal, Félix Sancenón, Ramón Martínez-Máñez,* and Mar Orzáez**

Acute lung injury (ALI) is a severe pulmonary disorder responsible for high percentage of mortality and morbidity in intensive care unit patients. Current treatments are ineffective, so the development of efficient and specific therapies is an unmet medical need. The activation of NLPR3 inflammasome during ALI produces the release of proinflammatory factors and pyroptosis, a proinflammatory form of cell death that contributes to lung damage spreading. Herein, it is demonstrated that modulating inflammasome activation through inhibition of ASC oligomerization by the recently described MM01 compound can be an alternative pharmacotherapy against ALI. Besides, the added efficacy of using a drug delivery nanosystem designed to target the inflamed lungs is determined. The MM01 drug is incorporated into mesoporous silica nanoparticles capped with a peptide (TNFR-MM01-MSNs) to target tumor necrosis factor receptor-1 (TNFR-1) to proinflammatory macrophages. The prepared nanoparticles can deliver the cargo in a controlled manner after the preferential uptake by proinflammatory macrophages and exhibit anti-inflammatory activity. Finally, the therapeutic effect of MM01 free or nanoparticulated to inhibit inflammatory response and lung injury is successfully demonstrated in lipopolysaccharide-mouse model of ALI. The results suggest the potential of pan-inflammasome inhibitors as candidates for ALI therapy and the use of nanoparticles for targeted lung delivery.

1. Introduction

Inflammatory pulmonary disorders are a major health concern due to the high morbidity and mortality in critical ill patients. In particular, acute lung injury (ALI) is an early phase of acute respiratory distress syndrome characterized by severe lung inflammatory response and pulmonary injury with mortality values that reach 39–46% of hospitalized patients.[1–4] The main treatments for ALI are focused on supportive therapies based on mechanical ventilation and pharmacological medication with corticosteroids.[5–7] Although many research efforts have been carried out in last years, the molecular and cellular mechanisms involved in ALI development still remain unclear and the effective prevention and treatment have not been successfully achieved.[8] The progression of the disease to the uncontrolled lung inflammation is regulated by the activated alveolar macrophages and aggravated by the associated proinflammatory cell death in the lung tissue.[9,10] In

A. García-Fernández, E. Garrido, F. Sancenón, R. Martínez-Máñez
Instituto Interuniversitario de Investigación de Reconocimiento Molecular y Desarrollo Tecnológico (IDM)
Universitat Politècnica de València
Universitat de València
Camí de vera s/n, Valencia 46022, Spain
E-mail: algarfe4@etsia.upv.es; rmaez@qim.upv.es

A. García-Fernández, E. Garrido, F. Sancenón, R. Martínez-Máñez
CIBER de Bioingeniería
Biomateriales y Nanomedicina (CIBER-BBN)
Av. Monforte de Lemos, 3-5, Madrid 28029, Spain

A. García-Fernández, M. Sancho, F. Sancenón, R. Martínez-Máñez, M. Orzáez
Unidad Mixta UPV-CIPF de Investigación en Mecanismos de Enfermedades y Nanomedicina
Universitat Politècnica de València
Centro de Investigación Príncipe Felipe
C/Eduardo Primo Yúfera 3
Valencia 46012, Spain
E-mail: morzaez@cipf.es

M. Sancho, V. Bisbal, M. Orzáez
Centro de Investigación Príncipe Felipe
Eduardo Primo Yúfera 3
Valencia 46012, Spain

M. Sancho, M. Orzáez
Departament de Bioquímica i Biologia Molecular
Universitat de València
Burjassot E-46100, Spain

F. Sancenón, R. Martínez-Máñez
Departamento de Química
Universitat Politècnica de València
Camino de Vera s/n
Valencia 46022, Spain

The ORCID identification number(s) for the author(s) of this article can be found under https://doi.org/10.1002/adhm.202301577

DOI: 10.1002/adhm.202301577

particular, interleukin-1β (IL-1β) is a key player in disease evolution being responsible of increased lung vascular permeability and pulmonary edema.[11] Recent studies have demonstrated the role of the NLR family pyridine domain 3 (NLPR3) inflammasome in ALI.[12–15] NLRP3 is an intracellular receptor from the innate immune system that, in response to diverse damage signals, binds to the adaptor apoptosis-associated speck-like protein containing a CARD domain (ASC) to finally recruit and activate the inflammatory protease procaspase-1. Once activated, caspase-1 cleaves pro-IL-1β and -18 to their active forms that are released from the cell contributing to inflammation.[16,17] Besides, caspase-1 also cleaves gasdermin D resulting in the formation of pores in the cellular membrane, which induces the proinflammatory form of cell death known as pyroptosis.[18,19] Due to the critical role of NLRP3 in the pathogenesis of ALI, the inflammasome key mediators have become promising pharmacological targets[13,20,21] and in recent years inhibitors of caspase-1 activity,[22,23] antagonists of interleukin-1 receptor,[24] and other anti-inflammatory compounds (such as flavonoids or antioxidants) have been analyzed in ALI animal models with positive results.[25–28] ALI development is a major determining factor of the prognosis of patients with severe acute respiratory syndrome coronavirus-2 (SARS-CoV-2) infection.[29] In addition, studies in COVID-19 patients indicate that disease severity correlates with an exacerbated inflammatory response in which ASC plays a role.[30] Interestingly, Rodrigues et al. reported that monocytes from SARS-CoV-2 infected patients exhibited increased ASC speck formation, NLRP3 inflammasome activation, and lactate dehydrogenase release compared to monocytes from healthy donors.[31]

An important related issue to be taken into account for the development of effective ALI treatments is the fact that the efficient delivery of drugs to the inflamed lungs is still an unresolved challenge.[32,33] In this scenario, the development of nanomedicines to target lungs in ALI has become an intensive area of research.[34,35] The use of nanoparticles as reservoirs provides an improvement in the bioavailability of the drug to target organs resulting in an enhanced therapeutic effect that usually results in minimizing drug toxicity. In the last years, several nanoparticulated systems based on organic polymers,[36,37] lipid nanocarriers,[38,39] and inorganic materials[40] have been developed to deliver drugs to treat ALI. However, among them mesoporous silica nanoparticles (MSNs) have been poorly studied for this application.[41] MSNs have been widely used in biomedicine due to their unique properties, such as high loading capacity, stability, biocompatibility, and easy surface functionalization.[42–45] Moreover, the possibility to functionalize the external surface of MSNs makes them excellent candidates for the preparation of gated materials, which displays cargo delivery only upon the presence of certain chemical, biochemical or physical stimuli.[46–49] Moreover, when working with nanoparticles one can take advantage of the intrinsic capacity of macrophages to take nanomaterials and transport them to the inflamed site of action.[50–53] This effect is known as the extravasation through leaky vasculature and inflammatory cell-mediated sequestration (ELVIS) mechanism. Besides, two additional properties of MSNs make them suitable nanocarriers for the design of nanomedicines for ALI treatment. One is the preferentially accumulation of MSNs in lungs, due to the large area of absorption of the lungs and the rich circulation and permeability,[54–56] and the other is the possibility of anchoring targeting (bio)molecules in the nanodevice to target selected cells/organs.[57] At this respect, the use of antibodies or peptides to target proinflammatory macrophages has been described and some examples have been reported in their use for ALI treatment.[58–61]

Dealing with ALI treatments, we have recently described the inflammasome inhibition features of a 1,3-dihydro-2*H*-indol-2-one derivative (MM01),[62] which interferes with ASC oligomerization and procaspase-1 recruitment and activation. One of the main advantages of this inhibitor is the point of action, which circumvents caspase-1 activation, thus producing the inhibition of IL-1β release and, more interestingly, interfering with pyroptosis. The use of this novel inhibitor can bring new insights in ALI therapy considering the lack of effectiveness of current treatments, mainly based in the application of mechanical ventilation or/and pharmacological treatments consisting in the use of vasoactive agents, such as inhaled nitric oxide, and corticoids (hydrocortisone, prednisolone, and dexamethasone) trying to limit the cytokine storm cascade.[63,64] Hence, MM01 blocks, in addition to cytokine storm, the proinflammatory signaling spread.[62] On the other hand, attending that the limitation of most of the pharmacological therapies is attributed to the difficulty of the drugs to reach the lungs, nanomaterials such MSNs could be a promising tool to achieve increased drug availability and efficacy, due to greater drug protection till drug delivery on the diseased lungs, allowing to reduce dosage and frequency and thus limiting undesired side effects.[41,65]

Here we report the use of MSNs loaded with MM01 and capped with a peptide (TNFR-MM01-MSNs) to target the TNFR-1 receptor in proinflammatory macrophages. Besides, the efficacy of the nanodevice is tested in an in vivo lipopolysaccharide (LPS)-induced ALI model. We demonstrated that blocking oligomerization of ASC protein upon inflammasome activation in vivo reduces levels of proinflammatory cytokines and levels of leukocyte infiltration in inflamed lungs. Moreover, attending to the fact that some therapies blocking inflammatory cytokines are only partially successful and the need to improve the drug biodistribution in lungs,[66–68] our results show that the combination of MM01 therapy with targeted nanodevices could become an attractive strategy to limit injury and inflammation in lungs in the future.

2. Results and Discussion

2.1. Synthesis, Characterization, and Cellular Biocompatibility of the Prepared Nanodevices

With the aim of developing alternative pharmaceuticals and better formulations to treat ALI, we synthesized a nanoformulation based on gated MSNs loaded with the novel inflammasome inhibitor MM01. MSNs were prepared using a

F. Sancenón, R. Martínez-Máñez
Unidad Mixta de Investigación en Nanomedicina y Sensores
Universitat Politècnica de València
IIS La Fe. Av. Fernando Abril Martorell
106 Torre A 7ª planta, Valencia 46026, Spain

well-known synthetic procedure that used cetyltrimethylammonium bromide as a structure-directing agent and TEOS as a silica source. The as-made MSNs were then calcined in order to remove the structure-directing agent from the pore voids. MSNs were loaded with rhodamine B or with MM01 and the external surface of the nanoparticles functionalized with (3-isocyanatopropyl)triethoxysilane (solids NCO-RhB-MSNs and NCO-MM01-MSNs). Finally, pores were capped upon the addition of TNFR1 peptide, which was linked onto the external surface through the formation of urea bonds. This synthetic procedure yielded the final nanoparticles TNFR-RhB-MSNs and TNFR-MM01-MSNs (**Figure 1**A). In both solids, the bulky anchored peptide plays a dual role as a capping ensemble and as a targeting ligand (vide infra).

The structural and textural properties of TNFR-RhB-MSNs, TNFR-MM01-MSNs, and the intermediary solids, obtained during the different synthesis steps, were characterized. The presence of ordered mesoporous scaffold in all the prepared nanoparticles was confirmed by powder X-ray diffraction, which showed the (100) reflection typical of mesoporous materials (Figure S1, Supporting Information). Transmission electron microscopy (TEM) images showed the spherical morphology of the prepared nanoparticles in which the pores were observed as alternate black and white stripes (Figure 1B). The textural properties were determined for calcined MSNs and TNFR-RhB-MSNs by N_2 adsorption–desorption isotherms (Figure S1, Supporting Information). MSNs presented a surface area of 954.88 m^2 g^{-1}, pore volume of 0.71 cm^3 g^{-1}, and pore size of 2.7 nm, whereas for TNFR-RhB-MSNs values of 436.39 m^2 g^{-1} and 0.33 cm^3 g^{-1} were obtained for the surface area and pore volume, respectively. The reduction of surface area and pore volume are ascribed to cargo loading inside the pores and functionalization of the external surface of the nanoparticles with the gatekeeper.

Dynamic light scattering measurements showed a marked increase in the hydrodynamic diameter of the nanoparticles after each functionalization steps (Figure 1C). In this respect, calcined MSNs presented a hydrodynamic diameter of 125 ± 33 nm which increased to 184 ± 9 nm and to 267 ± 27 for NCO-MM01-MSNs and TNFR-MM01-MSNs, respectively. Besides, the zeta potential of the calcined MSNs was −31 ± 2 that changed to 15 ± 1 and 16 ± 2 for NCO-MM01-MSNs and TNFR-MM01-MSNs, respectively. The same trend was observed for TNFR-RhB-MSNs nanoparticles in which the staring hydrodynamic diameter increases to 150 ± 8 and to 182 ± 14 nm for NCO-RhB-MSNs and TNFR-RhB-MSNs, with respective zeta potential values of 19 ± 2 and 11 ± 2 (Figure S2, Supporting Information). The amounts of cargo and gating peptide in TNFR-RhB-MSNs and TNFR-MM01-MSNs were determined using thermogravimetric and HPLC analysis. TNFR-RhB-MSNs nanoparticles contained 0.18 mmol g^{-1} SiO_2 of rhodamine B and 0.03 mmol g^{-1} SiO_2 of TNFR peptide. Finally, amounts of 72.5 μg mg^{-1} SiO_2 of **MM01** (loading efficiency) and 0.03 mmol g^{-1} SiO_2 of peptide were measured for TNFR-MM01-MSNs. All these results demonstrated the successful loading (with the dye or drug) and functionalization of the external surface of MSNs with the TNFR peptide as gating ensemble.

In a next step, to assess the possibility of using TNFR-MM01-MSNs, the stability of nanoparticles was evaluated. For this purpose, TNFR-MM01-MSNs were suspended in PBS (pH 7.4) for 1 month and TEM and dynamic light scattering measurements were carried out over time to determine both morphology and size of nanoparticles, which are parameters related with stability.[69–71] The size and morphology of nanoparticles measured immediately after their preparation were used as references. The obtained results are shown in Figure S3 of the Supporting Information. As could be seen, TEM images taken at different days (0, 1, 3, 7, 14, and 31) showed that the typical hexagonal pore network in the nanoparticles remained unchanged. However, as expected, after 1 month some degradation of the mesoporous silica framework was found, being this a crucial point for further clinical application.[72,73] Besides, DLS measurements showed an average nanoparticle diameter of 210 nm that was also maintained overtime. Overall, the obtained results show that the nanoparticles did not exhibit any significant change, thus confirming the good stability of the nanoparticles in suspension, which made them ideal vehicles for administration.

Finally, the correct capping and controlled cargo release was first tested using the dye-loaded TNFR-RhB-MSNs nanoparticles. Delivery studies were carried out in PBS at pH 7.4 (mimicking physiological conditions) and in the presence of protease enzymes (mimicking lysosomal extract of endocytic cellular compartments) and the obtained results are shown in Figure S2C of the Supporting Information. At pH 7.4 negligible rhodamine B release was observed (≈10% of the maximum release after 180 min). By contrast, a marked dye release was found in the presence of the lysosomal extract and ascribed to protease-induced hydrolysis of the capping peptide. These results confirmed the proper ability of TNFR peptide as capping ensemble. A similar result was observed for TNFR-MM01-MSNs. In this case zero MM01 release was observed in PBS, whereas a remarkable MM01 delivery was achieved in presence of protease enzyme (Figure 1F).

The biocompatibility of the nanoparticle scaffold by using dye-loaded nanoparticles TNFR-RhB-MSNs with THP-1 monocytes and the epithelial lung adenocarcinoma cell line A549 was evaluated at different concentrations at 24 h by the cell proliferation WST-1 assay (Figure 1G; Figure S4A, Supporting Information). Nanoparticles were well-tolerated by THP-1 and A549 cells at concentrations up to 150 μg mL^{-1} with viabilities in the 80–100% range. On the other hand, the potential ability of nanoparticle scaffold to activate the immune system (and therefore an inflammatory response) was assessed by measuring the inflammatory cell death pyroptosis by lactate dehydrogenase (LDH) activity assay in THP-1 and A549 cells. TNFR-RhB-MSNs were unable to activate inflammatory cell death in both lines and a nonsignificant LDH release was observed indicating the absence of cellular death by necrosis or pyroptosis (Figure 1H; Figure S5A, Supporting Information). This effect was also confirmed by evaluating the possible morphological changes of THP-1 cells and proinflammatory M1 macrophages by TEM analysis. The results did not show significant differences between control and nanoparticle-treated cells (Figure S6, Supporting Information). These results evidenced the biocompatibility of the capped mesoporous scaffold. Besides, the safety of the final nanoparticles, TNFR-MM01-MSNs were also confirmed in THP-1 cells by the WST-1 assay and LDH activity (Figure 1G,H). In addition, the

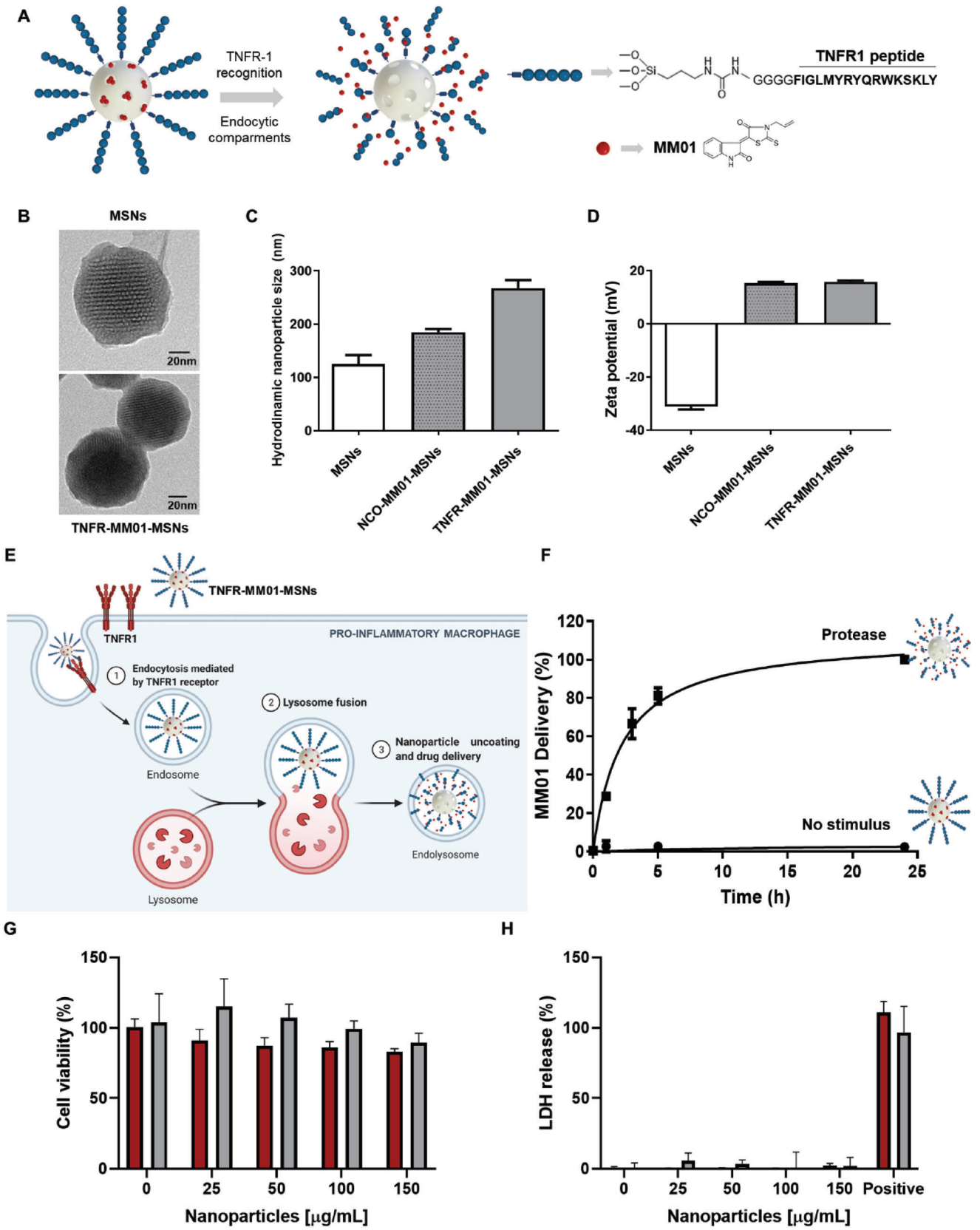

Figure 1. Synthesis and characterization of TNFR-RhB-MSNs and TNFR-MM01-MSNs. A) Representation of TNFR-MM01-MSNs design. B) TEM images of MSNs and TNFR-MM01-MSNs. C) Nanoparticle size of MSNs, NCO-MM01-MSNs, and TNFR-MM01-MSNs determined by dynamic light

safety of NCO-MM01-MSNs and TNFR peptide were evaluated discarding any possible toxic effect (Figure S5B, Supporting Information).

2.2. Cellular Uptake Studies in Proinflammatory M1 Macrophages

As explained above, the proinflammatory cytokine TNF-α has a relevant role in the outcome of pulmonary diseases and in particular in ALI.[74] The responsiveness of macrophages to the proinflammatory cytokine TNF-α depends on presence of the TNFR-1 and TNFR-2 receptors on the cellular surface. Binding of TNF-α to the TNFR-1 produces the activation of cell death signaling and contributes to inflammation. For these reasons, in a first step, we polarized (Figure S4, Supporting Information) and evaluated the presence of TNFR-1 receptor on the surface of THP-1 cells, M0 macrophages and proinflammatory M1 macrophages by western blot analysis. As could be seen in **Figure 2**A, proinflammatory M1 macrophages overexpress TNFR-1, making this cell surface receptor an appropriate candidate for targeting. In fact, recent reports demonstrated that an anti-TNFR-1 antibody prevents pulmonary inflammation in ALI, reinforcing the relevance of the TNFR-1 receptor in this lung disease model.[59,75] In this scenario, we aim using TNFR-MM01-MSNs to specifically target those activated macrophages that overexpress TNFR-1 and the intracellular release of the inflammasome inhibitor MM01 to eliminate their proinflammatory activity. To accomplish this objective, nanoparticles must be preferentially internalized by macrophages in a TNFR-1 dependent manner (Figure 2B). In order to study the selectivity of TNFR-RhB-MSNs nanoparticles (vide infra) a similar solid containing the same cargo but capped with a scrambled peptide (KKRSLFGSLLVVGAVTMGTLFWRKK) was prepared (Rd-RhB-MSNs). Cellular uptake and cargo release of both solids were tested by confocal microscopy and by flow cytometry. As could be seen in confocal images in Figure 2C, the intensity of the rhodamine fluorescence signal inside the inflammatory cells was significantly higher when using TNFR-RhB-MSNs than that observed in cells treated with Rd-RhB-MSNs. This preferential internalization of TNFR-RhB-MSNs was also assessed by flow cytometry (Figure 2D). Despite the Rd-RhB-MSNs can be endocyted by the cells, the presence of TNFR peptide onto the surface of MSNs favors the preferential internalization by receptor-mediated endocytosis. In accordance with this mechanism of action, the internalization of rhodamine-labeled TNFR-MSNs (TNFR-RhB*-MSNs) was reduced in proinflammatory macrophages preincubated with the endocytic inhibitor dynasore (≈10-fold) (Figure S9, Supporting Information) or in the presence of TNF-α that blocks TNFR (≈4-fold) (Figure S10, Supporting Information) where nanoparticles preferentially accumulate and colocalize with the cellular membrane. These results indicate that TNFR-1 peptide, anchored onto the external surface of TNFR-RhB-MSNs, selectively recognizes the TNFR-1 receptor, inducing a preferential internalization of TNFR-RhB-MSNs by M1 macrophages.

2.3. Cellular Studies of the Anti-Inflammatory Activity of TNFR-MM01-MSNs

To test the ability of MM01 and TNFR-MM01-MSNs to attenuate the inflammatory response in cellular models (**Figure 3**A), the NLPR3 inflammasome was stimulated in THP-1 monocytes and in proinflammatory M1 macrophages by activation with LPS and nigericin. Under these conditions, the activation of the inflammasome produces the cleavage of procaspase-1 to the active form caspase-1 that is secreted by the cell. As a consequence, the caspase-1 dependent processing of pro-IL-1β induced the subsequent release of IL1-β and an increment in the pyroptotic cell death that is reflected in an increased LDH activity, a typically intracellular enzyme, in the extracellular milieu. In a first step, the expression, processing, and secretion of the different components from the inflammasome activation cascade were analyzed (Figure 3B,C; Figures S7 and S8, Supporting Information). NLRP3 and caspase-1 protein expression in cell lysates was confirmed both in THP-1 monocytes and in M1 proinflammatory macrophages. The appearance of active caspase-1 in cell supernatants after LPS/nigericin treatment supports inflammasome activation. Interestingly, caspase-1 is reduced in the supernatants of cells treated with free MM01 and TNFR-MM01-MSNs, indicating that inhibition of the inflammasome is taking place upon treatment (Figure 3B,C). Finally, we also analyzed full-length gasdermin D (GSDMD), and the appearance of N-ter GSDMD fragment cleaved by caspase-1 responsible of pyroptosis. Upon inflammasome activation, the levels of full-length GSDMD decreased and the N-ter GSDMD fragment significantly increased. By contrast, TNFR-MM01-MSNs and free MM01 treatments induced a reduction of the N-ter GSDMD levels accompanied by a restoration of full-length GSDMD, as expected by inflammasome inhibition (Figure 3B,C).

In a second step, IL-1β levels and LDH activity in THP-1 cells (Figure 3D,F) and M1 macrophages (Figure 3E,G) were evaluated after treatment with TNFR-RhB-MSNs, TNFR-MM01-MSNs, and MM01. As could be seen, both THP-1 monocytes and M1 proinflammatory macrophages showed high levels of IL-1β and increased extracellular LDH activity after LPS/nigericin treatment. In the presence of TNFR-RhB-MSNs slightly changes in the IL-1β and LDH levels were observed. However, treatment with free MM01 or TNFR-MM01-MSNs reduced drastically the levels of IL-1β and the LDH activity. Both facts indicated that MM01 inhibits inflammasome activation as previously described[62] and in consequence, it causes the reduction of the IL-1β release and pyroptotic proinflammatory cell death that contributes to inflammation spreading. In addition, TNF-α was evaluated in both THP-1 cells and proinflammatory macrophages. As expected, no effect was observed in the downregulation of TNF-α

scattering. D) Zeta potential of MSNs, NCO-MM01-MSNs, and TNFR-MM01-MSNs. E) Schematic representation of TNFR-targeted nanoparticles uptake by proinflammatory macrophages and drug release. F) MM01 release profiles from TNFR-MM01-MSNs in PBS at pH 7.4 and in the presence of protease enzymes. G) Cell viability assays using TNFR-RhB-MSNs (red bars) and TNFR-MM01-MSNs (gray bars) in THP-1 cells by WST-1. H) Cellular death using LDH release assay in the presence of TNFR-RhB-MSNs and TNFR-MM01-MSNs. Positive control represents the lysate cells, which are correlated with the high inflammatory cell death. Data represent the means ± SEM of at least three independent experiments.

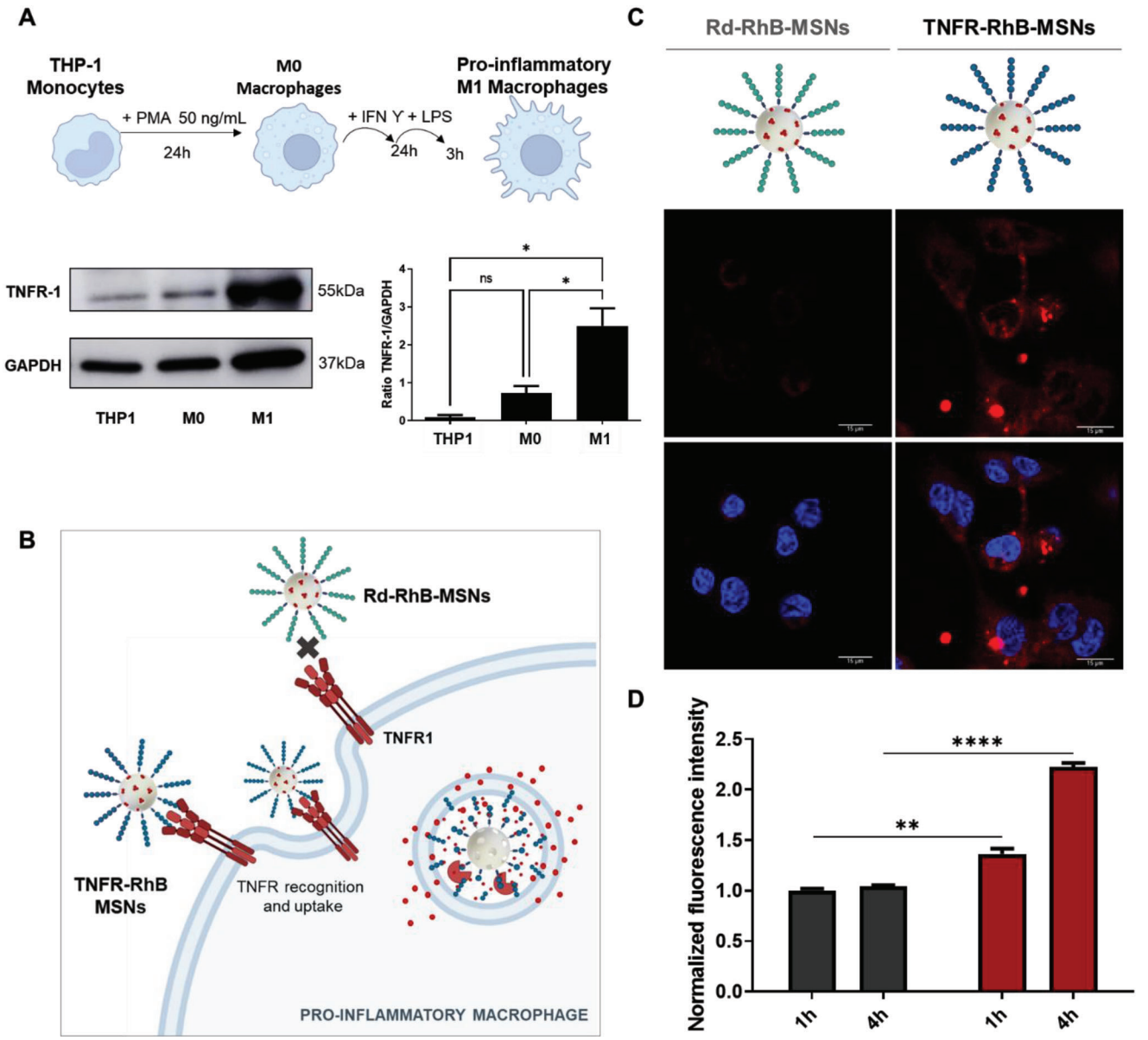

Figure 2. Targeting of TNFR-1 capped nanoparticles to M1 Macrophages. A) TNFR-1 expression profile in THP-1 monocytes, M0 macrophages, and proinflammatory M1 macrophages. B) Schematic representation of TNFR-1 recognition of TNFR-RhB-MSNs by proinflammatory macrophages compared to Rd-RhB-MSNs. C) Confocal images of proinflammatory M1 macrophages after treatment with Rd-RhB-MSNs (left) or TNFR-RhB-MSNs (right) for 4 h. Rhodamine B is represented in red and DNA marker Hoechst 33342 in blue. Scale bar corresponds to 15 µm. D) Rhodamine B intensity from proinflammatory M1 macrophages quantified by flow cytometry in the presence of Rd-RhB-MSNs (gray bars) or TNFR-RhB-MSNs (black bars) for 1 and 4 h. The data represent the means ± SEM of at least two independent experiments. Statistical analysis was performed by two-way ANOVA with multiple comparisons (**$p < 0.01$; **** $p < 0.0001$).

levels considering that MM01 does not interfere with the TNF-α activation pathway (Figure S11, Supporting Information). On the other hand, to evaluate the possible effect of TNFR peptide, proinflammatory macrophages were treated with TNFR-MM01-MSNs, NCO-MM01-MSNs, and free TNFR peptide (at equivalent concentration). NCO-MM01-MSNs results in a similar effect than TNFR-MM01-MSNs reducing the inflammatory response. The results showed a slight effect on the downregulation of the inflammatory response using the free peptide that can be correlated with the effect observed with TNFR-RhB-MSNs (see Figure S12, Supporting Information). This can be attributed to the TNFR peptide acting as a molecular gate that binds to the TNF receptor in the cellular membrane, and it could interact by blocking the receptor and thereby affecting the downregulation of the inflammatory cascade.[76,77] However, the effect is negligible and finally masked when combined with MM01, achieving in all cases a significant reduction of the cytokine's levels.

In addition, the obtained results indicate that MM01 encapsulated in TNFR-MM01-MSNs preserves its activity as an inflammasome modulator. In our experiments, a similar reduction

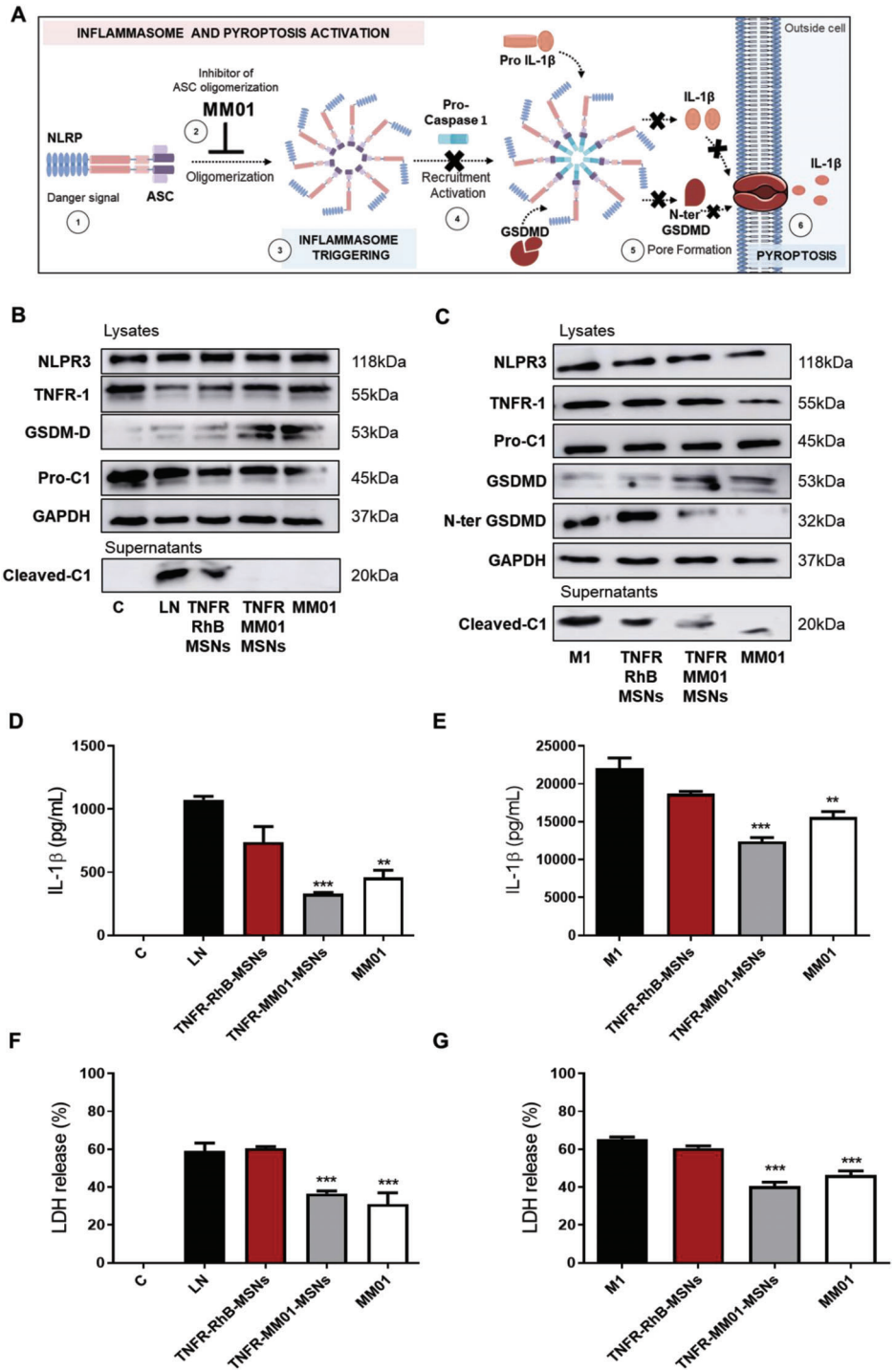

Figure 3. TNFR-MM01-MSNs inhibition of inflammasome in human monocytes and macrophages. A) Schematic representation of the MM01 mechanism of action. After a danger signal, NLRP-type receptors bind to the adaptor apoptosis-associated speck-like protein containing a CARD domain (ASC) (1). The application of MM01, that acts inhibiting ASC oligomerization (2) avoids inflammasome triggering (3) and thereby the subsequent impediment of procaspase-1 activation (4). The downstream inhibition of inflammatory cytokines, such as IL-1β and gasdermin D processing, respectively, avoids the pore formation in the cellular membrane (5), and thus inhibiting the proinflammatory cell death pyroptosis as well as inflammation spreading (6). Inflammatory studies with MM01, TNFR-RhB-MSNs, and TNFR-MM01-MSNs in THP-1 cells (left) and proinflammatory M1 macrophages (right). B,C) Western blot analysis of different proteins involved in the inflammatory response. Levels of cleaved caspase-1 were detected in cell supernatants and NLPR3, TNFR1, pro-Caspase 1, GSDMD, and N-ter GSDMD detected in cell lysates. GAPDH was used as a reference protein. D,E) Quantification of IL-1β proinflammatory cytokine from cell supernatants by ELISA. F,G) LDH release measured in cell supernatants as an inflammatory cell death marker of pyroptosis. Data represent the means ± SEM of at least three independent experiments. Statistical analysis was determined by one-way ANOVA (**$p < 0.01$; ***$p < 0.001$).

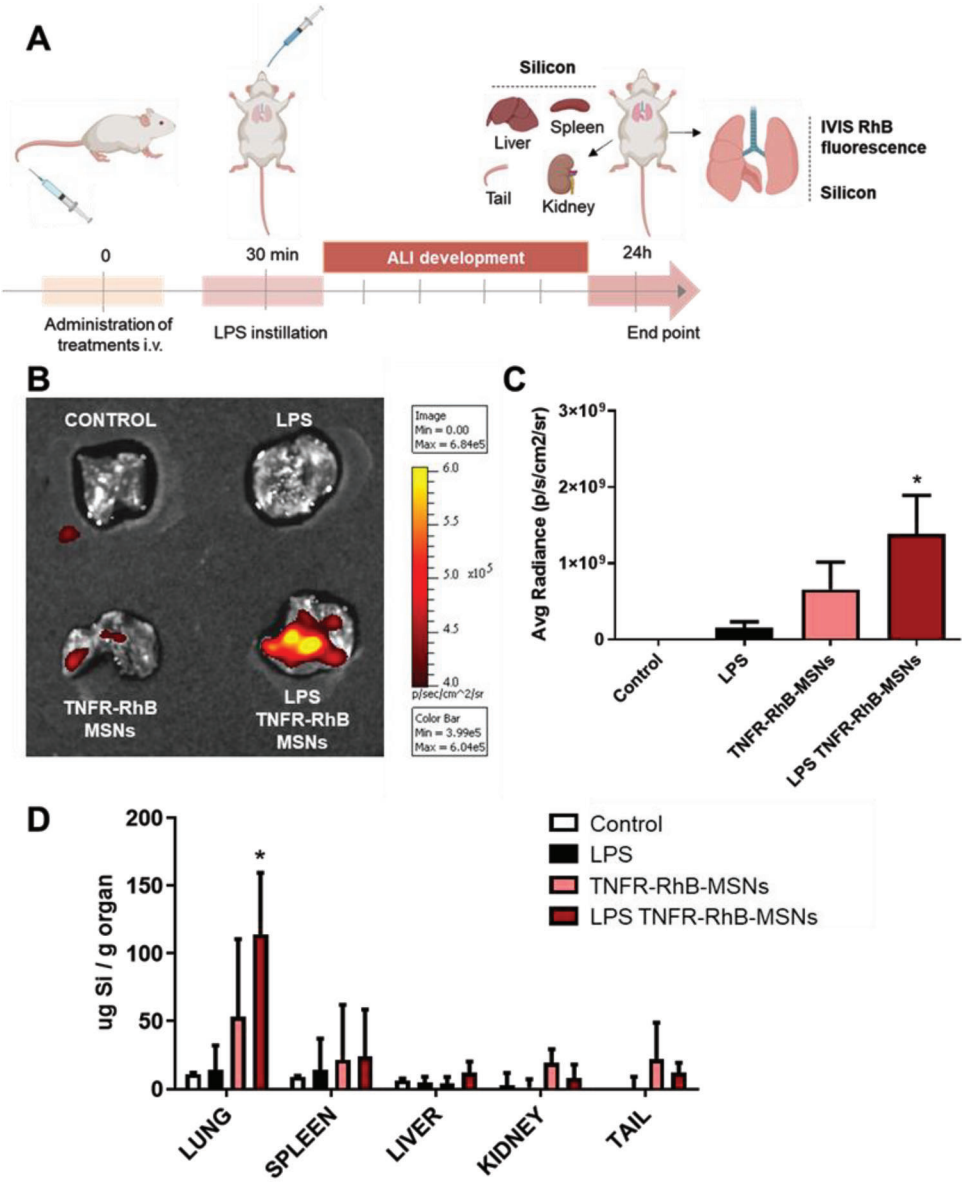

Figure 4. Targeting studies with TNFR-RhB-MSNs to inflamed lungs in an ALI mice model. A) Scheme of the ALI mice model for targeted studies. B) Representative lung images obtained using IVIS. C) Quantification of rhodamine B associated fluorescence. D) Biodistribution pattern of silicon in lung, liver, spleen, kidney, and tail. The graph showed the μg of silicon per gram of organ, measured by inductively coupled plasma mass spectroscopy (ICP-MS). The data represent the mean ± SEM and statistical significance was determined using a one-way ANOVA ($n = 4$). Statistical analysis was determined by applying two-way ANOVA with multiples comparisons (* $p < 0.05$).

in IL-1β and LDH levels was observed when using free MM01 or TNFR-MM01-MSNs, but the amount of the drug administered with the nanoformulation (6 μM) was 3.5-fold lower than that used with free MM01 (20 μM), which may increase the therapeutic window and avoid possible drug side effects. Additional advantages of the use of TNFR-MM01-MSNs nanoparticles for drug encapsulation are the recognition of alveolar proinflammatory macrophages mediated by the TNFR-1 targeting peptide and the potential passive targeting (ELVIS effect) that should be verified in in vivo settings (vide infra). Altogether the results suggest that the described delivery strategy could be a potential tool to avoid possible systemic effects derived from the anti-inflammatory systemic drug administration in vivo.

2.4. Targeted-Lung Delivery and Biocompatibility Profile of TNFR-MSNs for ALI Mice Model

To investigate the targeting ability of the TNFR-containing nanoparticles, TNFR-RhB-MSNs were used to track the accumulation of the nanoparticles in inflamed lungs in vivo in an ALI mice model (**Figure 4**A). In this model, the inflammation was induced by intratracheal instillation of LPS at semihigh doses

for 24 h. We monitored the presence of TNFR-RhB-MSNs in the lungs of animals either treated or not with LPS. 24 h after intravenous injection of nanoparticles, animals were sacrificed and rhodamine B accumulation in lungs was analyzed by quantifying fluorescence in an IVIS Spectrum (Figure 4B). A significant increase of fluorescence (quantification shown in Figure 4C) was observed in the lungs of animals cotreated with TNFR-RhB-MSNs and LPS when compared with control animals in which inflammation was not induced. The targeting ability of TNFR-RhB-MSNs to inflamed lungs was also studied by the determination of silicon levels, associated with the presence of nanoparticles, in selected organs. The higher silicon content was identified in the lungs of animals treated with LPS and TNFR-RhB-MSNs when compared to mice treated with TNFR-RhB-MSNs in the absence of inflammation (Figure 4D). These results confirmed the preferential targeting of TNFR-RhB-MSNs in inflamed lungs in an in vivo ALI model.

In parallel, the potential toxicity of TNFR-MM01-MSNs was evaluated in healthy CD-1 for the acute therapy according to the experimental protocol Guideline 423 of the Organization for Economic Cooperation and Development (OECD).[78] For this purpose, mice were treated with a single dose of TNFR-MM01-MSNs at 50 mg kg^{-1} (or vehicle) and were observed periodically for 15 days (**Figure 5**A). All animals survived the TNFR-MM01-MSNs treatment without any apparent affectation on their wellness or behavior (Figure 5B). Besides, histological analysis of the major organs (lungs, heart, liver, spleen, and kidney) did not reveal any evident pathological alteration, in terms of morphology and structure, in the treated animals compared to vehicle group (Figure 5C). Hemograms and biochemistry blood analytics corroborated the absence of alterations in the red and white blood cell lineages as well as proper renal and liver function (Figure S13, Supporting Information).

2.5. Anti-Inflammatory Activity of TNFR-MM01-MSNs In Vivo in an ALI Model

To study the therapeutic activity of MM01 in ALI, we analyzed different inflammatory parameters upon treatment of mice with free MM01 and TNFR-MM01-MSNs nanoparticles. Following established protocols, mice were treated with 10 mg kg^{-1} of MM01 or TNFR-MM01-MSNs at 50 mg kg^{-1} (equivalent to 3.6 mg kg^{-1} of MM01) and after 30 min animals were instilled intratracheally with LPS. The inflammatory profile and the effect of the treatments were evaluated after 24 h of LPS administration (**Figure 6**A).[40,79,80] The inflammatory response was analyzed by measuring the levels of proinflammatory cytokines (TNF-α, IL-6, and IL-1β) and the total amount of leukocytes in bronchoalveolar fluid (BALF) obtained from the lungs. Animals treated with MM01 or TNFR-MM01-MSNs showed significantly reduced levels of TNF-α, IL-6, and IL-1β (Figure 6B; Figure S15, Supporting Information). Moreover, after LPS treatment an increase of leukocytes was observed in BALF associated to the influx of inflammatory cells to injured lungs (Figure 6C). In comparison, in animals treated with MM01 and TNFR-MM01-MSNs, the leukocyte counts notably diminished (4.9- and 9.3-fold, respectively). The reduction was more evident in animals treated with TNFR-MM01-MSNs. In accordance with these results, evaluation of the systemic inflammatory parameters showed a reduced neutrophils/lymphocyte ratio in the case of animals treated with TNFR-MM01-MSNs when compared to free MM01 (Figure 6D,E), which is indicative of a better recovery from the inflammatory insult for animal treated with TNFR-MM01-MSNs.[60] We also found equivalent results in terms of inflammatory signaling between groups treated with only LPS or LPS + TNFR-RhB-MSNs, indicating that the nanoparticles did not induce any inflammatory response in the lungs.

Lung injury and recovery were also assessed by histological analysis, studying the alterations in alveolar tissue. Lung histology in ALI is mainly characterized by alveolar damage accompanied by interstitial thickening, neutrophil accumulation, formation of hyaline membranes, and other proteinaceous debris.[81,82] In our experimental setting, lung sections for healthy animals show thin alveolar walls, whereas clear disrupted lung architecture was observed in lungs from LPS treated mice (Figure 6F). Lung architecture was clearly restored in animals treated with MM01 and TNFR-MM01-MSNs (Figure 6F). Calculation of an ALI score following standard methods,[61] showed the highest punctuation for the LPS groups in which the strongest injury was produced, while the score significantly diminished in the animal groups treated with MM01 and TNFR-MM01-MSNs (Figure 6G). Despite some reports discuss the critical role of silica nanoparticles for lung therapy, related to safety issues, signs of lung damage or toxicity were discarded after the treatment with TNFR-RhB-MSNs confirming the biocompatibility of the nanodevice. Besides, specific markers were used to confirm the characteristic histological findings observed, such as the presence of neutrophils after LPS administration by myeloperoxidase activity staining (Figure S14, Supporting Information), to discard the fibrotic stage by Masson markers (Figure S16, Supporting Information), the increase of vascular inflammation by the VIII/Von Willebrand factor (Figure S17, Supporting Information) and the presence of alveolar proteinuria by the periodic acid Schiff (PAS) staining (Figure S18, Supporting Information).

Overall, our work demonstrates that MM01 inhibits the inflammatory response and lung injury in an LPS-mouse model of ALI. Moreover, their encapsulation in TNFR-MM01-MSNs allowed an improvement of the therapeutic effect of the free drug, mainly attributed to the direct drug delivery into the inflamed lungs with the subsequent nanoparticle uptake by TNFR1 overexpressed in proinflammatory macrophages.

3. Conclusion

The complexity of the ALI pathogenesis accompanied by the scarcity of useful treatments converts the study of new therapeutic alternatives in a medical need. In this work we successfully demonstrate the effectivity of the inflammasome inhibitor MM01 in the resolution of uncontrolled inflammation and lung injury in ALI. Interestingly, our in vivo model shares common features with other respiratory disorders, such those caused by SARS-CoV-2, which could validate the model for the study of this type of infections,[83] suggesting that the described efficacy of MM01 in ALI may be appropriate to COVID-19 therapy. Moreover, a nanodevice was prepared, based on mesoporous silica

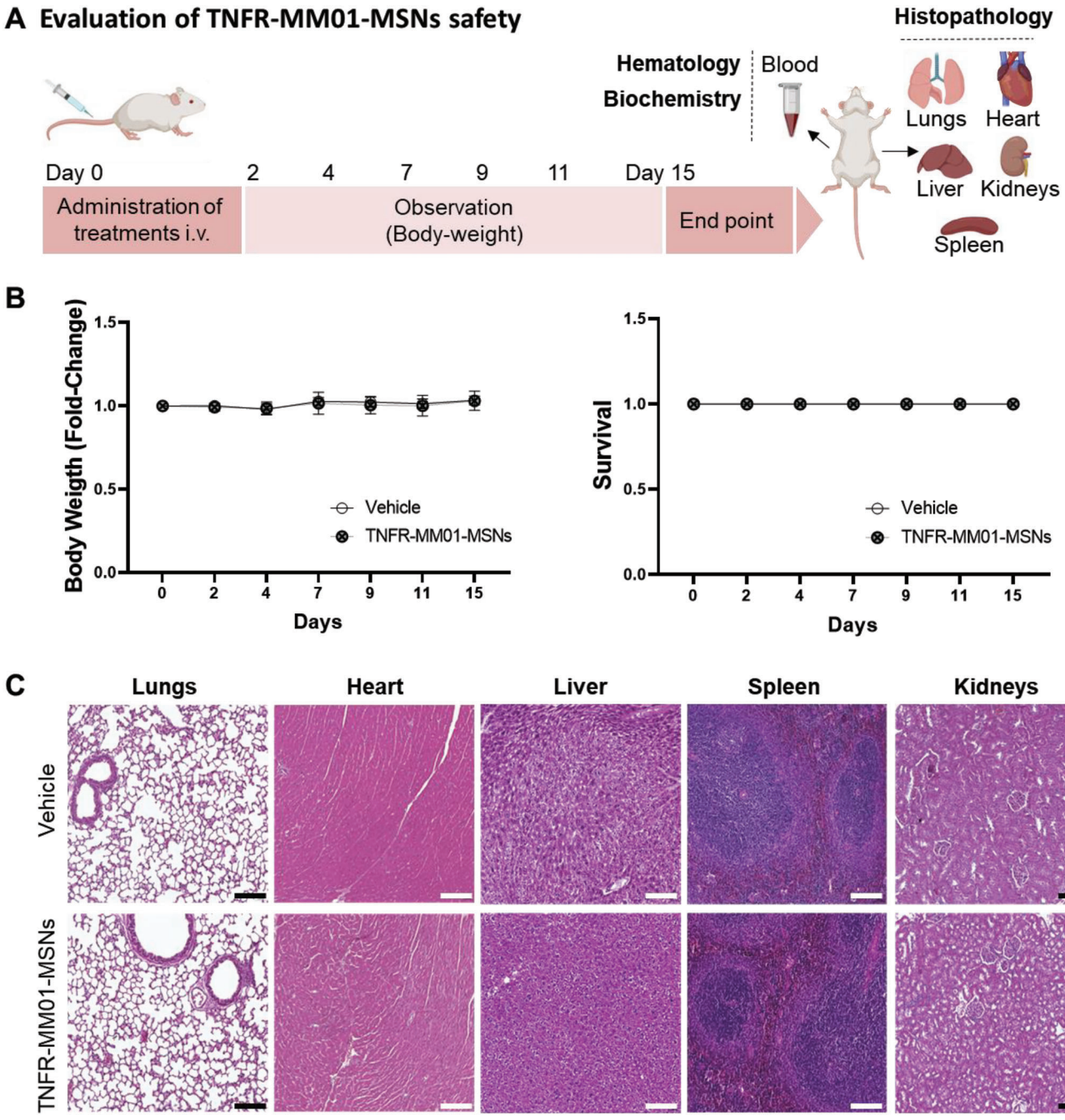

Figure 5. A) Acute systemic toxicity test. The behavior of healthy CD1 mice, vehicle or TNFR-MM01-MSNs (50 mg kg^{-1}) treated, was evaluated for 14 days ($n = 5$ per group). Then, blood and major organs were collected and biochemical, hematological, and histopathological changes were evaluated. B) Weight changes and survival in TNFR-MM01-MSNs toxicity assay for acute therapy. Data represents means ± SEM ($n = 5$ animals per group). C) Representative H&E staining images of main organs in treated mice with TNFR-MM01-MSNs after two weeks. Scale bar: 200 µm.

nanoparticles, loaded with the MM01 drug and capped with a TNFR targeting peptide (TNFR-MM01-MSNs). This work also describes, for the first time, the encapsulation of the drug MM01 as well as its proper activity after encapsulation into a MSNs scaffold and its application in both in vitro and in vivo models. Moreover, in concordance with previous reports that also support the use of targeted nanomedicines as promising approach for efficient drug delivery to inflamed lungs,[36,37,84–87] we demonstrate the targeting effect to inflamed lungs of TNFR-functionalized TNFR-RhB-MSNs by IVIS and silicon biodistribution analysis in ALI mice model. Targeted-delivery of MM01 using TNFR-MM01-MSNs also exhibited greater therapeutic effect of the entrapped drug. The nanoparticles allowed drug protection to the inflamed lungs, increasing its bioavailability and

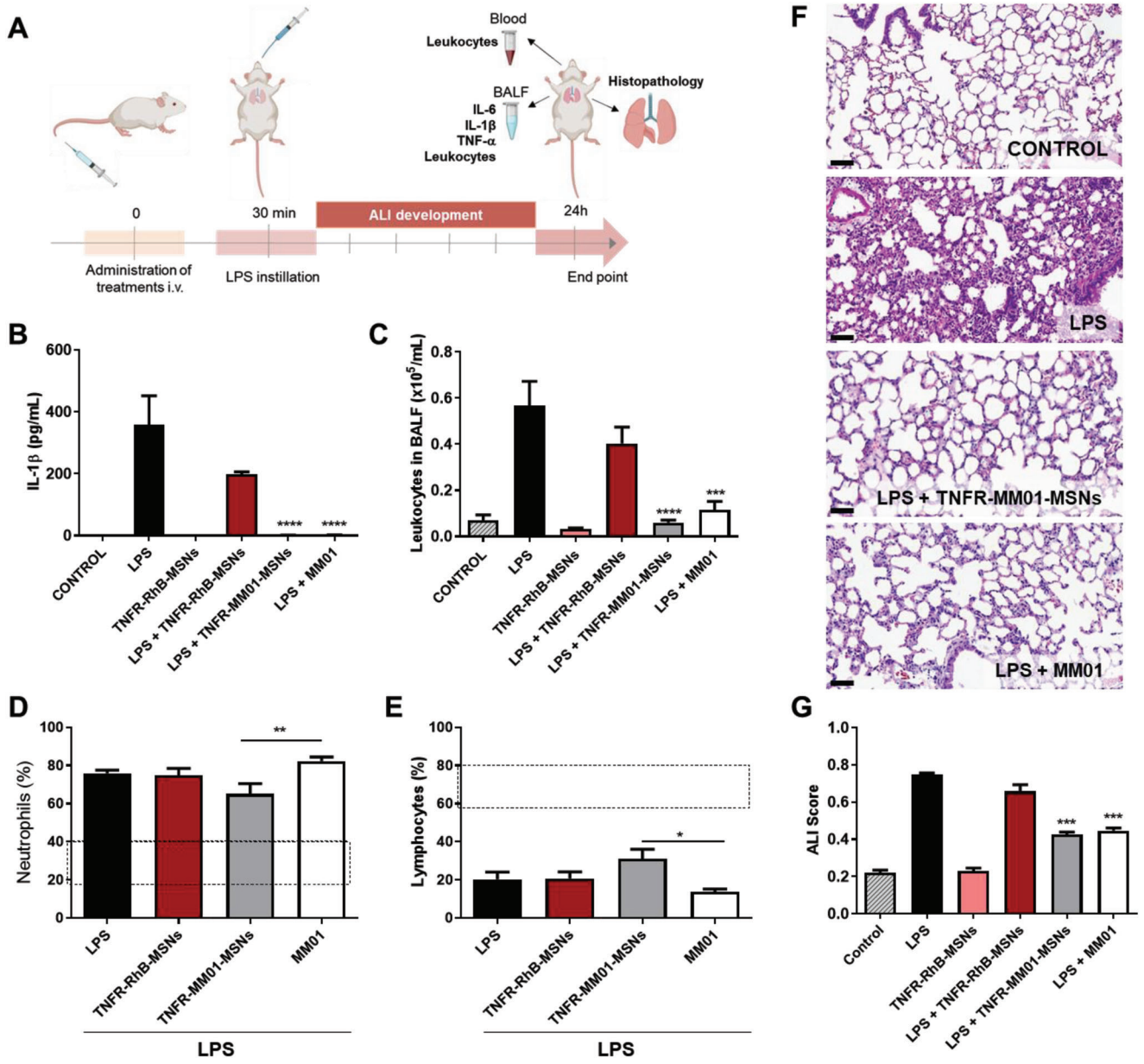

Figure 6. Anti-inflammatory activity of TNFR-MM01-MSNs in an ALI in vivo model. A) Schematic representation of ALI mice model for therapeutic evaluation. Female and male CD-1 mice (10–12 weeks of age) were distributed in six groups ($n = 10$). The acute lung injury was developed upon the LPS administration ((*E. coli* 055:B5, 2.5 mg kg^{-1}; i.t.) for 24 h. Prior to LPS administration the different treatments, TNFR-MM01-MSNs (50 mg kg^{-1}; equivalent to 3.6 mg kg^{-1} of MM01) and MM01 (10 mg kg^{-1}) were intravenously (i.v.) administered. B) Levels of IL-1β proinflammatory cytokine quantified by ELISA from BALF. C) Leukocytes account obtained from BALF by flow cytometry analysis, as indicator of inflammatory focus. D) Percentage of neutrophils and E) lymphocytes quantified from blood by flow cytometry analysis, as systemic inflammation indicators. The data represent the mean ± SEM. Statistics were determined by one-way ANOVA analysis (*$p < 0.05$; **$p < 0.01$; ***$p < 0.001$; ****$p < 0.0001$ compared to LPS group) ($n = 6$). F) Histopathological analysis of images H&E stain of lungs sections and G) evaluation of the acute lung injury determined by ALI score. Scale bar (in black) represents 50 µm. The data represent the mean ± SEM ($n = 4$). The data represent the mean ± SEM and statistical analysis was determined by applying one-way ANOVA (***$p < 0.001$; compared to LPS group).

thus efficacy, opening the possibility to reduce drug dosage or frequency in further therapy due to the direct lung delivery. The results confirmed that the combination of nanomedicine and a new pharmacological strategy could be an attractive approach to limit injury and inflammation in ALI, which could help to overcome clinical limitations of current treatments. Besides, our results suggest that mesoporous silica-based nanomedicines are a potential tool to efficiently administer anti-inflammatory drugs to solve other inflammatory disorders such as Chronic Pulmonary Obstructive Disease, asthma, pulmonary fibrosis, and COVID-19, which are also major health concerns in the clinics.

4. Experimental Section

Synthesis of MSNs: A CTABr solution in deionized water (1 g, 2.74 mmol) was prepared and then NaOH (3.5 mL, 2 M) was added. The solution was stirred, and the temperature adjusted to 80 °C. Then TEOS (5 mL, 2.57×10^{-2} mol) was added dropwise to yield the as-made MSNs. The final mixture was stirred for 2 h yielding a white precipitate, which was isolated by centrifugation and washed until neutral pH with deionized H_2O. The material was dried, and the final MSNs were obtained after calcination process at 550 °C in an oxidant atmosphere to remove the surfactant template.

Synthesis of NCO-RhB-MSNs: For MSNs loading, 38.32 mg of rhodamine B (0.8 mmol g^{-1} solid) was suspended in anhydrous CH_3CN (10 mL) and stirred overnight at room temperature. Then (3-isocyanatepropyl)triethoxysilane (124.93 µL, 5 mmol g^{-1} solid) was added and the suspension stirred 5.5 h in order to functionalize the external surface of MSNs. The solid was isolated by centrifugation, washed with CH_3CN, and dried at 37 °C obtaining a pink solid.

Synthesis of TNFR-RhB-MSNs: The TNFR-1 peptide (GGGGFIGLMYRYQRWKSKLY) was covalently attached onto the grafted MSNs through the formation of urea bonds. For this purpose, NCO-RhB-MSNs (30 mg) were suspended in CH_3CN (2 mL). On the other hand, a solution of the peptide (30 mg) was prepared in H_2O (2 mL) and added to the nanoparticles suspension together with triethylamine (80 µL). The mixture was stirred at room temperature for 2 h and then the solid was isolated by centrifugation, washed with water and with PBS. Finally, the final solid was dried at 37 °C.

Synthesis of TNFR-RhB-MSNs*: Rhodamine B isothiocyanate (RBIT, 1 mg) was reacted with (3-aminopropyl)triethoxysilane (APTES, 10 µL) in anhydrous acetonitrile (3 mL). The mixture was stirred in the dark overnight at room temperature. Then MSNs (5 mg) were dispersed in anhydrous acetonitrile (2.5 mL) and the RBIT/APTES mixture (20 µL) was added with 3.1 µL of (3-isocyanatopropyl)triethoxysilane (2.5 mmol g^{-1} solid). The suspension was left in the dark for 5.5 h at room temperature. Nanoparticles were washed with acetonitrile and dried to yield NCO-RhB*-MSNs. To obtain TNFR-RhB*-MSNs, 1 mg of labeled nanoparticles were stirred in acetonitrile (0.2 mL), and a suspension of TNFR (1 mg in 0.2 mL of water) and TEA (2 µL) were added. The mixture was incubated for 2 h at room temperature and then the solid was washed with water and PBS and dried to yield TNFR-RhB*-MSNs.

Synthesis of NCO-MM01-MSNs: The pores of the MSNs were loaded with MM01 (Merck R639036) using an impregnation method. For this purpose, a saturated solution of MM01 (26 mg in 1 mL of DMSO) was prepared and separated in two aliquots. 50 mg of MSNs was extended on a plate and a first 500 µL of MM01 suspension was added dropwise. The mixture was dried at 37 °C and then a second cycle of impregnation was carried out. The MM01-loaded MSNs were obtained after drying the solid at 37 °C. Then, the loaded nanoparticles were suspended in anhydrous CH_3CN and an excess of (3-isocyanatepropyl)triethoxysilane (32.48 µL, 5 mmol g^{-1} solid) was added to the suspension. The solid was stirred at room temperature for 5.5 h and then was collected by centrifugation, washed with CH_3CN, and dried at 37 °C to obtain NCO-MM01-MSNs. Taking into account the amount of MM01 used for NCO-MM01-MSNs preparation and the final content determined by HPLC measurements in the nanoparticles, an entrapment efficiency of ≈20% was calculated.

Synthesis of TNFR-MM01-MSNs: The TNFR-1 peptide (40 mg) was dissolved in H_2O (2 mL) and then added to the NCO-MM01-MSNs suspension (40 mg in 2 mL of CH_3CN). Finally, triethylamine (80 µL) was added and the mixture was stirred at room temperature for 2 h. The resulting solid was obtained by centrifugation, washed with water and PBS, and finally, dried at 37 °C to yield TNFR-MM01-MSNs.

Characterization Procedures: The prepared materials were characterized by standard techniques. Powder X-ray diffraction patterns were obtained on a Seifert 3000TT diffractometer using Cu Kα radiation. TEM images were obtained in a Philips CM-10. Micromeritics ASAP2010 automated sorption analyzer was used to record N_2 adsorption–desorption isotherms. Thermogravimetric analyses were performed on a TGA/SDTA 851e Mettler Toledo equipment, using an oxidant atmosphere (Air, 80 mL min^{-1}) with a heating program consisting on a heating ramp of 10 °C per min from 393 to 1273 K and an isothermal heating step at this temperature for 30 min. HPLC studies were carried out with a Merck Hitachi L-2130 HPLC pump, an L-2200 autosampler and a Lichrospher100 C18 (150 × 3.9 mm) column using gradients of CH_3CN-H_2O with 0.1% TFA as the mobile phase.

TNFR-MM01-MSNs Stability Assay: In order to assess the stability of the nanoparticles a suspension of 1.5 mg of TNFR-MM01-MSNs in PBS (pH 7.4) was prepared and monitored during 1 month. At different times (0, 1, 3, 7, 14, and 31 days) dynamic light scattering measurements and TEM analysis were carried out.

Drug Delivery Studies: To evaluate the capping features of TNFR1 peptide, TNFR-RhB-MSNs were suspended in PBS at pH 7.4 (mimicking physiological conditions) or in lysosomal extract at pH 5 (to mimic endocytic cellular compartments). Lysosomal extract was purified from animal tissues in accordance to Lysosome Isolation Kit (LYSISO1; Sigma-Aldrich) following the provided instructions. To perform the delivery studies, 1 mg of the nanoparticles was suspended in 2 mL of PBS or 2 mL of lysosomal extract and stirred at 37 °C, respectively. At scheduled times aliquots were isolated by centrifugation and dye release was followed by the fluorescence emission band of rhodamine B at 575 nm (λ_{ex} = 555 nm).

To evaluate MM01 delivery from TNFR-MM01-MSNs, 1 mg of the nanoparticles was suspended in 400 µL of H_2O at pH 7.4 and stirred at 37 °C. Both samples were centrifuged for 5 min at 12 000 rpm and the absorbance (λ_{exc} = 325 nm) of the supernatant (120 µL) was measured to obtain the initial point. This volume was returned to the corresponding aliquot. After that, 2 mg of protease enzyme (final concentration of 5 mg mL^{-1}) was added to one of the aliquots. Both suspensions were stirred at 37 °C. Then, after a certain time interval 120 µL of supernatant was taken from both suspensions, treated, and measured as above. This procedure was repeated until it allowed to construct the release kinetics of the capped material in both, absence, and presence of the protease enzyme.

Cell Culture Conditions: A549 cell line was obtained from ATCC and maintained in DMEM supplemented with 10% of FBS at 37 °C in an atmosphere of 5% carbon dioxide and 95% air. Human leukemic monocyte THP-1 cells were obtained from the German Resource Centre for Biological Materials (DSMZ) and were maintained in RPMI-1640 supplemented with 10% of FBS at 37 °C in an atmosphere of 5% carbon dioxide and 95% air. For macrophage polarization from THP-1 cells (M0), 800 000 cells mL^{-1} was seeded in a 6-well plate and derived into nonpolarized macrophages with the addition of 50 ng mL^{-1} phorbol 12-myristate 13-acetate (PMA; Sigma-Aldrich) for 24 h of incubation in RPMI medium. Then, medium was replaced with complete RPMI 1640 supplemented with 1% FBS to differentiate macrophages to proinflammatory (M1). For M1 polarization, 20 ng mL^{-1} of interferon-ϒ (IFN-ϒ; Invitrogen) was added and cells were incubated for 24 h, and finally incubated with LPS (100 ng mL^{-1}; Sigma-Aldrich) for 3 h.

TNFR-1 Characterization in Proinflammatory Macrophages: To confirm the TNFR-1 expression profile, western blot analyses in the different inflammatory cells were performed. For this purpose, THP-1 cells were cultured and polarized to M0 macrophages and M1 proinflammatory macrophages as described above. Whole cell extracts were obtained by scrape-collecting in 50 µL of lysis buffer (25 mM Tris-HCl pH 7.4, 1 mM EDTA, 1 mM EGTA, and 1% SDS plus protease and phosphatase inhibitors). Lysates were separated by SDS-PAGE electrophoresis, transferred to nitrocellulose membranes, blocked with 5% nonfat milk and incubated with TNFR-1 antibody (C25C1 from Cell Signalling) overnight. GAPDH expression (MA5-15738 from Invitrogen) was also analyzed in cell lysates as reference protein for normalization. Membranes were washed and incubated with horseradish peroxidase-conjugated secondary antibody. Chemiluminescent signal was detected using Amersham Imager 600 instrument.

Cytotoxicity Cell Studies: The cytotoxic effect of nanoparticle scaffold was assessed in biocompatibility studies measuring cell proliferation activity by Cell Proliferation Reagent WST-1 assay (11644807001 from Merck) and inflammatory cell-death pyroptosis by LDH activity assay (Promega, Ref. J2381). For this purpose, THP-1 and lung A549 cells were seeded in a 96-well plate and treated with TNFR-RhB-MSNs at 0, 25, 50, 100, and

150 μg mL^{-1} for 24 h. To determine cell viability, WST-1 was added and after 1 h absorbance at 595 nm was registered in a Wallac 1420 workstation. For LDH activity measurement, cell supernatants were collected following the manufacturer's instructions. In parallel, the possible toxic effect of the nanoparticles in terms of morphological changes in the cells was evaluated through transmission electron microscopy. For this purpose, THP-1 cells or proinflammatory macrophages cells were seeded in chamber slides for 24 h and incubated with nanoparticles for 24 h. Then, cells were washed and fixed with 3% of glutaraldehyde in sodium phosphate buffer (0.1 M), dehydrated in ethanol, and stained with uranyl acetate (1%) and osmium tetroxide (1%). The samples were included in epoxy resin (Araldite) to obtain sections for TEM analysis. TEM images were acquired using a microscope FEI Tecnai Spirit G2 operating at 80 kV with a digital camera (Soft Image System, Morada). Besides, to evaluate the possible toxic effect of the final nanoparticles WST-1 cell viability and LDH-release assays were carried out in THP-1. The cells were incubated with TNFR-MM01-MSNs, NCO-MM01-MSNs, and TNFR peptide at different concentrations for 24 h. Nanoparticles were used at 0, 25, 50, 100, and 150 μg mL^{-1} and an equivalent concentration of TNFR peptide attached to the nanoparticles was used in a free solution (0, 1.25, 2.5, 5, and 10 μg mL^{-1}).

Targeted Cellular Uptake Studies: The cellular uptake TNFR-MSNs was studied using rhodamine B-labeled nanoparticles (TNFR-RhB*-MSNs). Proinflammatory macrophages were seeded on glass coverslips in 6-well plates and incubated at 37 °C for 24 h. Then, cells were incubated with the nanoparticles (50 μg mL^{-1}) for 1 h in the absence or presence of the endocytic inhibitor (Dynasore 100 μM). Then, slides were washed, DNA marker (2 μg mL^{-1}, Hoechst 33342) and cellular membrane marker (5 μg mL^{-1}, Wheat Germ Agglutinin Alexa Fluor 647 Conjugate, Invitrogen Ref. W32466) were added, and slides were visualized under a confocal microscope Leica TCS SP8 HyVolution II. Besides, activated macrophages (seeded on glass coverslips in 6-well plates) were treated with TNF-α (1 ng mL^{-1}) for 1 h to block the TNFR receptor. Then macrophages were treated with TNFR-RhB*-MSNs (50 μg mL^{-1}) for 1 h. Then, slides were washed and visualized by confocal microscopy in the presence of Hoechst 33342 (2 μg mL^{-1}) and Wheat Germ Agglutinin Alexa Fluor 647 Conjugate (5 μg mL^{-1}). The images were analyzed using ImageJ to determine the cellular uptake by means of positive cells.

The added effect of active targeting of the TNFR-RhB-MSNs was evaluated in THP-1 cells and polarized proinflammatory (M1) macrophages by confocal microscopy and flow cytometry studies. Moreover, to confirm the selectivity of TNFR-RhN-MSNs, a similar solid containing a scrambled-peptide sequence (Rd-RhB-MSNs) was prepared. THP-1 cells were seeded in a 6-well plate and polarized to M1 macrophages as previously described. Then, flow cytometry studies were carried out to determine the nanoparticles uptake by the inflammatory cells. THP-1 monocytes and M1 macrophages were treated with TNFR-RhB-MSNs and Rd-RhB-MSNs solids (50 μg mL^{-1}) and, after 30 min, cells were washed with PBS and media replaced to remove the noninternalized nanoparticles. Then, cells were incubated for a total time of 1 and 4 h, respectively. Finally, cells were washed and collected for rhodamine B detection by flow cytometry. The single-cell fluorescence determinations were realized using CytoFLEX S instrument (Beckman-Coulter, USA) and analyzed in the CytoFLEX software. Nanoparticle internalization was confirmed in THP-1 cells and proinflammatory (M1) macrophages by confocal microscopy. For this purpose, cells were seeded over glass-cover slips in 6-well plates and treated with TNFR-RhB-MSNs and Rd-RhB-MSNs (50 μg mL^{-1}) for 30 min. Then noninternalized nanoparticles were removed by replacing media and cells were incubated for a total time of 1 and 4 h. Next, cells were washed with PBS and Hoechst 33342 nuclei stain was added at 2 μg mL^{-1}. The fluorescence signal was followed using a Leica TCS SP8 confocal microscope.

Anti-Inflammatory Activity of TNFR-MM01-MSNs in Inflammatory Cells: The anti-inflammatory activity of TNFR-MM01-MSNs was studied in the proinflammatory (M1) macrophages and in THP-1 cells. In the case of THP-1, cells were seeded in a 6-well plate at 800 000 cells mL^{-1} in RPMI 1% FBS and incubated for 24 h. Then, cells were treated with TNFR-MM01-MSNs at 25 μg mL^{-1} suspended in PBS (being an equivalent dose of 6 μM of **MM01**) and free-formulated MM01 was added at 20 μM in DMSO as reference. Moreover, TNFR-RhB-MSNs (25 μg mL^{-1}) were used as control. As an additional control, the possible effect of TNFR peptide (1.25 μg mL^{-1}, equivalent dose to nanoparticles) and NCO-MM01-MSNs (25 μg mL^{-1}) was also evaluated in proinflammatory macrophages. After 30 min of treatments, LPS from *Escherichia coli* (100 ng mL^{-1}) was added for 3 h and nigericin (Sigma-Aldrich) at 20 μM during the last 30 min of incubation to activate the NLPR3 inflammasome. In the case of proinflammatory (M1) macrophages, THP-1 was derived with PMA as described above and after 24 h of incubation, media were replaced for RPMI 1% FBS and IFN-Υ at 20 ng mL^{-1} was added for 24 h. Then, treatments were added in a similar manner as THP-1 cells. After 30 min of the addition, LPS from *E. coli* (100 ng mL^{-1}) was added for 3 h and nigericin (10 μM) during the last 30 min of incubation.

The activity of TNFR-MM01-MSNs was examined by measuring the amount of IL-1β and TNF-α secreted in the cell culture supernatants of inflammatory cells by ELISA kit following supplier's instructions (Human IL-1β ELISA Set II (Ref. 557953) and Human TNF ELISA Set (Ref. 555212) from BD Biosciences). In addition, LDH activity was measured in cell supernatants to determine the pyroptosis cell death using the LDH Assay Kit II following manufacturer instructions. Finally, the inflammasome components were characterized by western blot analysis both in cell lysates and supernatants from THP-1 cells and proinflammatory (M1) macrophages. The proteins studied in cell lysate were NLPR3, TNFR-1, pro-Caspase-1, pro-Gasdermin D (GSDMD), N-ter Gasdermin D, and GAPDH as protein reference to normalize the expression levels. In cell supernatants, cleaved Caspase-1 (p20) was analyzed. Whole extracts were obtained from cells using a lysis buffer (25 mM Tris-HCl pH 7.4, 1 mM EDTA, 1 mM EGTA, and 1% SDS plus protease and phosphatase inhibitors) and supernatants samples were collected and concentrate by lyophilization. The samples were separated by SDS-PAGE, transferred to nitrocellulose membranes, blocked with 5% nonfat milk and incubated with the different primary antibody in each case (see the Supporting Information) overnight at 4 °C. Finally, membranes were incubated with horseradish peroxidase secondary antibody and chemiluminescence detection was carried out in Amersham Imager 600 instrument.

Animal Studies: Female and male CD-1 mice (10–12 weeks of age) were obtained from Charles River (France) and were maintained in a temperature-controlled room with a 12 h light/dark cycle with access to food and water. The study was approved by the Ethical Committee for Animal Experiments at Centro de Investigación Príncipe Felipe (Valencia, Spain) in strict accordance with the Ethical Committee for Research and Animal Welfare Generalitat Valenciana, Conselleria d'Àgricultura, Medi ambient, Canvi climatic I Desenvolupmanet Rural (2018/VSP/PEA/0094).

To evaluate the toxicity of the TNFR-MM01-MSNs for acute lung injury therapy the experimental protocol Guideline 423 of the OECD was followed. Healthy female and male CD1 mice were randomly distributed into two groups of five animals. The animals were treated with a single dose of the nanoparticles (50 mg kg^{-1} in PBS) or vehicle and were observed periodically during the next 15 days. Considering the effective therapeutic activity for MM01 was determined at 10 mg kg^{-1} in previous studies, the nanoaprticle dose was fixed according to the equivalent concentration of encapsulated MM01. After that, animals were euthanized and blood extraction and dissection of different organs were obtained to examine the possible toxicity through clinical analysis (haematology and biochemistry) and histopathology. The organs were fixed with 4% paraformaldehyde and then included in paraffin, cut with a microtome into 2 μm sections, placed on coated glass slides and stained by hematoxylin and eosin (H&E) for histological evaluation. The Leica ASP300 tissue processor was used to register the slides and the analysis was performed with the CaseViewer software.

To evaluate the activity of TNFR-MM01-MSNs in the ALI model mice, six groups of ten animals were used including male and female mice. The different groups were 1) control, 2) LPS treated, 3) administered with TNF-RhB-MSNs, 4) treated with LPS + TNFR-RhB-MSNs, 5) administered with LPS + TNFR-MM01-MSNs and, 6) treated with LPS + MM01. The acute lung injury (ALI) was established upon LPS (*E. coli* 055:B5, 2.5 mg kg^{-1}) intratracheal instillation in 50 μL of saline for 24 h. Prior to LPS administration, the nanoparticles TNFR-MM01-MSNs were administered intravenously by tail vein injection at 50 mg kg^{-1} in 200 μL of PBS, being

equivalent of 3.6 mg kg^{-1} of free formulated MM01. The free drug was administered at 10 mg kg^{-1} in 200 µL of PBS and PBS vehicle was administered in the control and LPS animals. Moreover, TNFR-RhB-MSNs were administered at 50 mg kg^{-1} as nanoparticle control in 200 µL of PBS. For LPS instillation, the animals were previously anesthetized with ketamine (75 mg kg^{-1}) and dexmedetomidine (1 mg kg^{-1}) and then anaesthesia was reverted using 1 mg kg^{-1} of atipamezole. After 24 h of ALI development, the animals were euthanized with overdose of sodium pentobarbital. Bronchoalveolar lavage fluid (BALF), blood extraction, and dissection of different organs were realized to examine the inflammatory response and pulmonary injury.

BALF Analysis: For BALF obtention six of the ten animals per group to perform a lung lavage using intratracheal injections of 250 µL of PBS. BALF was collected and centrifuged at 1200 rpm for 5 min at 4 °C to separate supernatant from cells. The cell pellet was suspended in PBS and total leukocyte number was analyzed by flow cytometry by Acvlab (Valencia). BALF supernatants were used to measure the expression of TNF-α, IL-6, and IL-1β cytokines using ELISA kit following the supplier's instructions. Finally, the total protein expression in BALF was determined by BCA protein assay kit.

Histopathology Analysis of ALI Score: Lungs from four of the ten animals were selected and embedded with 4% paraformaldehyde. After this treatment, lungs were fixed in paraffin, cut with a microtome into 2 µm sections, placed on coated glass slides and stained by hematoxylin and eosin for histological evaluation to determine the ALI Score. The Leica ASP300 tissue processor was used to register the slides and the analysis was performed with the CaseViewer software. For ALI score evaluation, at least 20 random high-power fields were independently examined for each group. ALI score was examined in different gradations attending to mainly histological findings (neutrophils in the alveolar space, neutrophils in the interstitial space, hyaline membranes, proteinaceous debris filling the airspaces and alveolar septal thickening). In addition, the sections were analyzed with different markers to evaluate the neutrophil presence by myeloperoxidase activity, the determination of alveolar proteinosis evaluating the accumulation of carbohydrates using PAS stainer, the fibrosis development using Masson's trichrome to analyze the deposition of collagen and the vascular inflammation by factor VIII/Von Willebrand factor staining.

TNFR-RhB-MSNs Biodistribution in ALI Mouse Model: The targeting features to inflamed lungs of TNFR-RhB-MSNs were confirmed in vivo monitoring the rhodamine B fluorescence in an IVIS spectrum imaging system (PerkinElmer Inc.). For this purpose, the lungs from four animals from each group to obtain IVIS images were used. The lungs were harvested after the euthanasia and immediately analyzed in the IVIS equipment using excitation wavelength of 535 nm and emission wavelength of 580 nm. In addition, the silicon presence, associated to MSNs, was quantified in selected organs (lungs, liver, kidneys, spleen, and tail) by ICP-MS. The samples were digested with 1 mL of 25% tetramethylammonium hydroxide into polytetrafluorethylene tubes. The digestion process was established at 80 °C for 2 h using a Bloc Digest 20 (Selecta). Finally, samples were diluted to 10 mL of water and filtered to measure Si in 7900 ICP-MS system in H_2 mode using germanium as an internal standard.

Statistical Analysis: All the values represent the mean ± SEM of at least three independent experiments except the in vivo experiment with mice in which a single representative experiment is shown ($n = 10$ animals per group). For in vivo studies, mice were randomly assigned to treatment groups; the sample size was not predetermined. Significance was determined by one-way ANOVA followed by Tukey's post tests or by two-way ANOVA with multiple comparisons with Tukey's post tests using GraphPad 8 software. A p-value below 0.05 was considered statistically significant and indicated with an asterisk: ($*p < 0.05$; $**p < 0.01$; $***p < 0.001$; $****p < 0.0001$).

Supporting Information

Supporting Information is available from the Wiley Online Library or from the author.

Acknowledgements

This research was supported by Project Nos. PID2021-126304OB-C41, PID2021-128141OB-C22, and PID2020-115048RB-I00 funded by MCIN/AEI/10.13039/501100011033 and by European Regional Development Fund – A way of doing Europe. The authors also thank Generalitat Valenciana (PROMETEO Project CIPROM/2021/007 and PROMETEO 2019/065) for support. E.G. is grateful to the Spanish MIU and European Union-Next Generation EU for her "Margarita Salas" postdoctoral grant (UP2021-036). The authors would also like to thank Animal Facilities from Centro de Investigación Principe Felipe for its support in the animal research and procedures, and I. Borred and J. Forteza from Instituto Valenciano de Patología for its technical support in the histopathology analysis. The authors thank for the use of Biorender.com in the figures and graphical abstract.

Conflict of Interest

The authors declare no conflict of interest.

Data Availability Statement

The data that support the findings of this study are available from the corresponding author upon reasonable request.

Keywords

acute lung injury, mesoporous silica nanoparticles, MM01, targeted-lung delivery

Received: May 16, 2023
Revised: July 14, 2023
Published online: August 12, 2023

[1] G. R. Bernard, A. Artigas, K. L. Brigham, J. Carlet, K. Falke, L. Hudson, M. Lamy, J. R. Legall, A. Morris, R. Spragg, *Am. J. Respir. Crit. Care Med.* **1994**, *149*, 818.
[2] M. A. Matthay, R. L. Zemans, G. A. Zimmerman, Y. M. Arabi, J. R. Beitler, A. Mercat, M. Herridge, A. G. Randolph, C. S. Calfee, *Nat. Rev. Dis. Primers* **2019**, *5*, 18.
[3] W.-J. Gu, Y.-D. Wan, H.-T. Tie, Q.-C. Kan, T.-W. Sun, *PLoS One* **2014**, *9*, 90426.
[4] J. F. Avecillas, A. X. Freire, A. C. Arroliga, *Clin. Chest Med.* **2006**, *27*, 549.
[5] M. Cepkova, M. A. Matthay, *J. Intensive Care Med.* **2006**, *21*, 119.
[6] E. R. Johnson, M. A. Matthay, *J. Aerosol Med. Pulm. Drug Delivery* **2010**, *23*, 243.
[7] G. A. Schmidt, *Clin. Chest Med.* **2016**, *37*, 647.
[8] Y. Butt, A. Kurdowska, T. C. Allen, *Arch. Pathol. Lab. Med.* **2016**, *140*, 345.
[9] P. A. Ward, *Eur. Respir. J.* **2003**, *22*, 22.
[10] M. A. Matthay, R. L. Zemans, *Annu. Rev. Pathol.: Mech. Dis.* **2011**, *6*, 147.
[11] M. T. Ganter, J. Roux, B. Miyazawa, M. Howard, J. A. Frank, G. Su, D. Sheppard, S. M. Violette, P. H. Weinreb, G. S. Horan, M. A. Matthay, J.-F. Pittet, *Circ. Res.* **2008**, *102*, 804.
[12] X. He, Y. Qian, Z. Li, E. K. Fan, Y. Li, L. Wu, T. R. Billiar, M. A. Wilson, X. Shi, J. Fan, *Sci. Rep.* **2016**, *6*, 31663.
[13] J. J. Grailer, B. A. Canning, M. Kalbitz, M. D. Haggadone, R. M. Dhond, A. V. Andjelkovic, F. S. Zetoune, P. A. Ward, *J. Immunol.* **2014**, *192*, 5974.

[14] D. Jiang, J. Liang, J. Fan, S. Yu, S. Chen, Y. Luo, G. D. Prestwich, M. M. Mascarenhas, H. G. Garg, D. A. Quinn, R. J. Homer, D. R. Goldstein, R. Bucala, P. J. Lee, R. Medzhitov, P. W. Noble, *Nat. Med.* **2005**, *11*, 1173.
[15] M. Leissinger, R. Kulkarni, R. L. Zemans, G. P. Downey, S. Jeyaseelan, *Am. J. Respir. Crit. Care Med.* **2014**, *189*, 1461.
[16] K. Schroder, J. Tschopp, *Cell* **2010**, *140*, 821.
[17] L. Franchi, T. Eigenbrod, R. Muñoz-Planillo, G. Nuñez, *Nat. Immunol.* **2009**, *10*, 241.
[18] X. Liu, Z. Zhang, J. Ruan, Y. Pan, V. G. Magupalli, H. Wu, J. Lieberman, *Nature* **2016**, *535*, 153.
[19] J. Shi, Y. Zhao, K. Wang, X. Shi, Y. Wang, H. Huang, Y. Zhuang, T. Cai, F. Wang, F. Shao, *Nature* **2015**, *526*, 660.
[20] D. Li, W. Ren, Z. Jiang, L. Zhu, *Mol. Med. Rep.* **2018**, *18*, 5427.
[21] N. R. Aggarwal, L. S. King, F. R. D'Alessio, *Am. J. Physiol.* **2014**, *306*, L709.
[22] G. Mathiak, G. Grass, T. Herzmann, T. Luebke, C. C. Zetina, S. A. Boehm, H. Bohlen, L. F. Neville, A. H. Hoelscher, *Br. J. Pharmacol.* **2000**, *131*, 383.
[23] D.-D. Wu, P.-H. Pan, B. Liu, X.-L. Su, L.-M. Zhang, H.-Y. Tan, Z. Cao, Z.-R. Zhou, H.-T. Li, H.-S. Li, L. Huang, Y.-Y. Li, *China Med. J. (Engl.)* **2015**, *128*.
[24] P. Gasse, C. Mary, I. Guenon, N. Noulin, S. Charron, S. Schnyder-Candrian, B. Schnyder, S. Akira, V. F. J. Quesniaux, V. Lagente, B. Ryffel, I. Couillin, *J. Clin. Invest.* **2007**, *117*, 3786.
[25] D. Impellizzeri, G. Bruschetta, E. Esposito, S. Cuzzocrea, *Expert Opin. Emerging Drugs* **2015**, *20*, 75.
[26] V. J. Patel;, H. J. Metha, M. Joo, R. T. Sadikot, *Biomed Res. Int.* **2018**, *2018*, 2476824.
[27] M. Shyamsundar, S. T. W. McKeown, C. M. O'Kane, T. R. Craig, V. Brown, D. R. Thickett, M. A. Matthay, C. C. Taggart, J. T. Backman, J. S. Elborn, D. F. McAuley, *Am. J. Respir. Crit. Care Med.* **2009**, *179*, 1107.
[28] H. J. Lago, C. A. Toledo-Arruda, M. Mernak, H. K. Barrosa, A. M. Martins, F. I. Tibério, M. C. Prado, *Molecules* **2014**, *19*, 3570.
[29] L. Li, Q. Huang, D. C. Wang, D. H. Ingbar, X. Wang, *Clin. Transl. Med.* **2020**, *10*, 20.
[30] S. Toldo, R. Bussani, V. Nuzzi, A. Bonaventura, A. G. Mauro, A. Cannatà, R. Pillappa, G. Sinagra, P. Nana-Sinkam, P. Sime, A. Abbate, *Inflamm. Res.* **2021**, *70*, 7.
[31] T. S. Rodrigues, K. S. G. de Sá, A. Y. Ishimoto, A. Becerra, S. Oliveira, L. Almeida, A. V. Gonçalves, D. B. Perucello, W. A. Andrade, R. Castro, F. P. Veras, J. E. Toller-Kawahisa, D. C. Nascimento, M. H. F. de Lima, C. M. S. Silva, D. B. Caetite, R. B. Martins, I. A. Castro, M. C. Pontelli, F. C. de Barros, N. B. do Amaral, M. C. Giannini, L. P. Bonjorno, M. I. F. Lopes, R. C. Santana, F. C. Vilar, M. Auxiliadora-Martins, R. Luppino-Assad, S. C. L. de Almeida, F. R. de Oliveira, et al., *J. Exp. Med.* **2021**, *218*, 20201707.
[32] S. P. Newman, *Ther. Delivery* **2017**, *8*, 647.
[33] R. T. Sadikot, A. V. Kolanjiyil, C. Kleinstreuer, I. Rubinstein, *Biomed Hub.* **2017**, *477086*, 3570.
[34] R. Iyer, C. C. W. Hsia, K. T. Nguyen, *Curr. Pharm. Des.* **2015**, *21*, 5233.
[35] M. M. Bailey, C. J. Berkland, *Med. Res. Rev.* **2009**, *29*, 196.
[36] A. Bohr, N. Tsapis, I. Andreana, A. Chamarat, C. Foged, C. Delomenie, M. Noiray, N. El Brahmi, J. Majoral, S. Mignani, E. Fattal, *Biomacromolecules* **2017**, *18*, 2379.
[37] C. Y. Zhang, W. Lin, J. Gao, X. Shi, M. Davaritouchaee, A. E. Nielsen, R. J. Mancini, Z. Wang, *ACS Appl. Mater. Interfaces* **2019**, *11*, 16380.
[38] S. Jiang, S. Li, J. Hu, X. Xu, X. Wang, X. Kang, J. Qi, X. Lu, J. Wu, Y. Du, Y. Xiao, *Nanomed.: Nanotechnol. Biol. Med.* **2019**, *15*, 25.
[39] S.-J. Li, X.-J. Wang, J.-B. Hu, X.-Q. Kang, L. Chen, X.-L. Xu, X.-Y. Ying, S.-P. Jiang, Y.-Z. Du, *Drug Delivery* **2017**, *24*, 402.
[40] Y. Xiong, W. Gao, F. Xia, Y. Sun, L. Sun, L. Wang, S. Ben, S. E. Turvey, H. Yang, Q. Li, *Adv. Healthcare Mater.* **2018**, *7*, 1800510.
[41] A. García-Fernández, F. Sancenón, R. Martínez-Máñez, *Adv. Drug Delivery Rev.* **2021**, *177*, 113953.
[42] F. Tang, L. Li, D. Chen, *Adv. Mater.* **2012**, *24*, 1504.
[43] A. Watermann, J. Brieger, *Nanomaterials* **2017**, *7*, 189/1.
[44] S. T. Haque, E. H. Chowdhury, *Curr. Drug Delivery* **2018**, *15*, 485.
[45] A. García-Fernández, E. Aznar, R. Martínez-Máñez, F. Sancenón, *Small* **2020**, *16*, 1902242.
[46] C. Coll, A. Bernardos, R. Martínez-Máñez, F. Sancenón, *Acc. Chem. Res.* **2013**, *46*, 339.
[47] E. Aznar, M. Oroval, L. Pascual, J. R. Murguía, R. Martínez-Máñez, F. Sancenón, *Chem. Rev.* **2016**, *116*, 561.
[48] X. Pu, J. Li, P. Qiao, M. Li, H. Wang, L. Zong, Q. Yuan, S. Duan, *Curr. Cancer Drug Targets* **2019**, *19*, 285.
[49] A. Llopis-Lorente, B. Lozano-Torres, A. Bernardos, R. Martínez-Máñez, F. Sancenón, *J. Mater. Chem. B* **2017**, *5*, 3069.
[50] A. García-Fernández, G. García-Laínez, M. L. Ferrándiz, E. Aznar, F. Sancenón, M. J. Alcaraz, J. R. Murguía, M. D. Marcos, R. Martínez-Máñez, A. M. Costero, M. Orzáez, *J. Controlled Release* **2017**, *248*, 60.
[51] E. Koziolová, K. Venclíkova, T. Etrych, *Physiol. Rev.* **2018**, *67*, S281.
[52] C. A. Fromen, W. J. Kelley, M. B. Fish, R. Adili, M. J. Hoenerho, M. Holinstat, O. Eniola-Adefeso, *Bioeng. Transl. Med.* **2017**, *1*, 10797.
[53] F. Yuan, L. Quan, L. Cui, S. R. Goldring, D. Wang, *Adv. Drug Delivery Rev.* **2012**, *64*, 1205.
[54] T. Wu, M. Tang, *J. Appl. Toxicol.* **2018**, *38*, 25.
[55] T. Yu, D. Hubbard, A. Ray, H. Ghandehari, *J. Controlled Release* **2012**, *163*, 46.
[56] Y. Chen, H. Chen, J. Shi, *Adv. Mater.* **2013**, *25*, 3144.
[57] L. Pascual, C. Cerqueira-Coutinho, A. García-Fernández, B. de Luis, E. S. Bernardes, M. S. Albernaz, S. Missailidis, R. Martínez-Máñez, R. Santos-Oliveira, M. Orzaez, F. Sancenón, *Nanomed.: Nanotechnol. Biol. Med.* **2017**, *13*, 2495.
[58] D. Hristodorov, R. Mladenov, V. Von Felbert, M. Huhn, R. Fischer, S. Barth, T. Thepen, D. Hristodorov, R. Mladenov, V. Von Felbert, M. Huhn, R. Fischer, S. Barth, *mAbs* **2015**, *7*, 853.
[59] Y. Weifeng, L. Li, H. Yujie, L. Weifeng, G. Zhenhui, H. Wenjie, *PLoS One* **2016**,*11*, e0151672.
[60] M. M. M. Chronic, O. A. Akinrinmade, S. Chetty, A. K. Daramola, M. Islam, T. Thepen, S. Barth, *Biomedicines.* **2017**, *5*, 56.
[61] A. García-Fernández, M. Sancho, V. Bisbal, P. Amorós, M. D. Marcos, M. Orzáez, F. Sancenón, R. Martínez-Máñez, *J. Controlled Release* **2021**, *337*, 14.
[62] P. M. Soriano-Teruel, G. García-Laínez, M. Marco-Salvador, J. Pardo, M. Arias, C. DeFord, I. Merfort, M. J. Vicent, P. Pelegrín, M. Sancho, M. Orzáez, *Cell Death Dis.* **2021**, *12*, 1155.
[63] F. Lamontagne, M. Briel, G. H. Guyatt, D. J. Cook, N. Bhatnagar, M. Meade, *J. Crit. Care* **2010**, *25*, 420.
[64] K. Raghavendran, G. S. Pryhuber, P. R. Chess, B. A. Davidson, P. R. Knight, R. H. Notter, *Curr. Med. Chem.* **2008**, *15*, 1911.
[65] J. S. Brenner, *Ann. Am. Thorac. Soc.* **2017**, *14*, 561.
[66] M. A. Matthay, D. F. McAuley, L. B. Ware, *Lancet Respir. Med.* **2017**, *5*, 524.
[67] Z. Zhang, L. Chen, H. Ni, *Sci. Rep.* **2015**, *5*, 17654.
[68] J. V. Diaz, R. Brower, C. S. Calfee, M. A. Matthay, *Crit. Care Med.* **2010**, *38*, 1644.
[69] Y.-S. Lin, N. Abadeer, C. L. Haynes, *Chem. Commun.* **2011**, *47*, 532.
[70] K. Yoncheva, B. Tzankov, M. Popova, V. Petrova, N. Lambov, *J. Dispersion Sci. Technol.* **2016**, *37*, 113.
[71] M. Kaasalainen, V. Aseyev, E. von Haartman, D. Ş. Karaman, E. Mäkilä, H. Tenhu, J. Rosenholm, J. Salonen, *Nanoscale Res. Lett.* **2017**, *12*, 74.
[72] J. G. Croissant, Y. Fatieiev, N. M. Khashab, *Adv. Mater.* **2017**, *29*, 1604634.
[73] K. Braun, A. Pochert, M. Beck, R. Fiedler, J. Gruber, M. Lindén, *J. Sol-Gel Sci. Technol.* **2016**, *79*, 319.

[74] S. Mukhopadhyay, J. R. Hoidal, T. K. Mukherjee, *Respir. Res.* **2006**, *7*, 125.
[75] M. R. Wilson, K. Wakabayashi, S. Bertok, C. M. Oakley, R. Lucas, J. Mcguire, *Front. Immunol.* **2017**, *8*, 1.
[76] A. D'Alessio, M. S. Kluger, J. H. Li, R. Al-Lamki, J. R. Bradley, J. S. Pober, *J. Biol. Chem.* **2010**, *285*, 23868.
[77] D. Brenner, H. Blaser, T. W. Mak, *Nat. Rev. Immunol.* **2015**, *15*, 362.
[78] OECD, *Test No. 423 : Acute Oral Toxicity – Acute Toxic Class Method*, OECDGuidelines for Testing of Chemicals, Section 4, OECD Publishing, Paris **2002**.
[79] L. Wang, Y. Rao, X. Liu, L. Sun, J. Gong, H. Zhang, L. Shen, A. Bao, H. Yang, *J. Nanobiotechnol.* **2021**, *19*, 56.
[80] L. Sun, Y. Liu, X. Liu, R. Wang, J. Gong, A. Saferali, W. Gao, A. Ma, H. Ma, S. E. Turvey, S.-Y. Fung, H. Yang, *Adv. Sci.* **2022**, *9*, 2104051.
[81] Y. A. P. A. Sato, K. Gonda, M. Harada, Y. Tanisaka, S. Arai, Y. Mashimo, H. Iwano, H. Sato, S.- Ryozawa, T. Takahashi, S. Sakuramoto, M. Shibata, *Biomed. Rep.* **2017**, *7*, 79.
[82] G. Matute-bello, G. Downey, B. B. Moore, S. D. Groshong, M. A. Matthay, *Am. J. Respir. Cell Mol. Biol.* **2010**, *44*, 725.
[83] B. Al-Ani, A. M. ShamsEldeen, S. S. Kamar, M. A. Haidara, F. Al-Hashem, M. Y. Alshahrani, A. M. Al-Hakami, D. H. A. Kader, A. Maarouf, *Clin. Exp. Pharmacol. Physiol.* **2022**, *49*, 483.
[84] S. H. van Rijt, D. A. Bölükbas, C. Argyo, K. Wipplinger, M. Naureen, S. Datz, O. Eickelberg, S. Meiners, T. Bein, O. Schmid, T. Stoeger, *Nanoscale* **2016**, *8*, 8058.
[85] S. Hussain, Z. Ji, A. J. Taylor, L. M. Degra, M. George, C. J. Tucker, C. H. Chang, R. Li, J. C. Bonner, S. Garantziotis, *ACS Nano.* **2016**, *10*, 7675.
[86] M. Bouchoucha, E. Beliveau, F. Kleitz, F. Calon, M.-A. Fortin, *J. Mater. Chem. B* **2017**, *5*, 7721.
[87] M. Santha Moorthy, G. Hoang, B. Subramanian, N. Q. Bui, M. Panchanathan, S. Mondal, V. P. Thi Tuong, H. Kim, J. Oh, *J. Mater. Chem. B* **2018**, *6*, 5220.